
Benchmarking Out-of-Distribution Generalization Capabilities of DNN-based Encoding Models for the Ventral Visual Cortex.

Spandan Madan
Harvard University

Will Xiao
Harvard Medical School

Mingran Cao
Francis Crick Institute

Hanspeter Pfister
Harvard University

Margaret Livingstone
Harvard Medical School

Gabriel Kreiman
Harvard Medical School

Abstract

We characterized the generalization capabilities of DNN-based encoding models when predicting neuronal responses from the visual cortex. We collected *Macaque-ITBench*, a large-scale dataset of neural population responses from the macaque inferior temporal (IT) cortex to over 300,000 images, comprising 8,233 unique natural images presented to seven monkeys over 109 sessions. Using *Macaque-ITBench*, we investigated the impact of distribution shifts on models predicting neural activity by dividing the images into Out-Of-Distribution (OOD) train and test splits. The OOD splits included several different image-computable types including image contrast, hue, intensity, temperature, and saturation. Compared to the performance on in-distribution test images—the conventional way these models have been evaluated—models performed worse at predicting neuronal responses to out-of-distribution images, retaining as little as 20% of the performance on in-distribution test images. The generalization performance under OOD shifts can be well accounted by a simple image similarity metric—the cosine distance between image representations extracted from a pre-trained object recognition model is a strong predictor of neural predictivity under different distribution shifts. The dataset of images, neuronal firing rate recordings, and computational benchmarks are hosted publicly at: [MacaqueITBench Link](#).

1 Introduction

Deep Neural Networks (DNNs) for vision have internal representations that share similarities with neural representations in the visual cortex, including the primate ventral visual stream [2, 3]. This representational similarity allows for models that use image representations extracted from a pre-trained DNN (e.g., ResNet [4]) to predict neuronal firing rates [5] (Fig. 1(a)). However, DNNs are known to struggle with generalization under distribution shifts such as Out-of-Distribution (OOD) viewpoints [6–8], materials and lighting [9, 10], and noise [11, 12]. This difficulty in generalization may also affect models of the visual cortex that rely on a DNN to extract image representations.

We posit that, even within an image set where DNN-based models predict neural responses well under random splits across images, specific train-test splits with distribution shifts will impair model performance, proportional to the size of distribution shift. To test this hypothesis, we collected *MacaqueITBench*, a large-scale dataset of responses to natural images by neurons in the macaque ventral visual pathway. The dataset represents neurons in V2, V4, Central IT (CIT), and Anterior IT (AIT) (primarily CIT and AIT) and responses to over 300,000 images (8,233 unique images presented to seven monkeys over 109 sessions), as illustrated in Fig. 1(b).

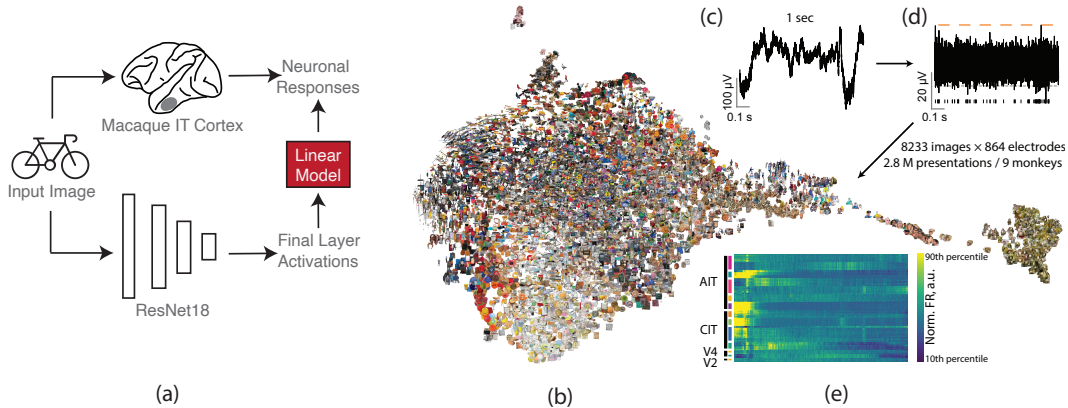


Figure 1: *Modeling the visual cortex with MacaqueITBench*. (a) DNN-Based models of the visual cortex employ a linear model to map image features extracted from pre-trained DNNs (e.g., ResNet18) to neuronal responses collected from the macaque IT cortex. (b) A UMAP [1] visualization of the representation by the neural pseudo-population. Nearby images have more similar population responses. (c) An example one-second segment of the raw wideband signals recorded on an electrode. (d), The wideband signals were highpass filtered, and threshold-crossing events below a voltage value (horizontal dashed line) were counted as multiunit spikes (lower vertical ticks). The top horizontal bars indicate image presentation periods. (e) The heatmap shows the neural response matrix. Each row indicates the responses from an electrode, pooled across sessions. The columns correspond to images, sorted by the reverse UMAP horizontal order. The vertical bars to the left of the heatmap denote the recorded areas (black lines) and monkeys (colored lines).

Using *MacaqueITBench*, we investigated the impact of distribution shifts on the neural predictivity of DNN-based models of the visual cortex. We constructed various OOD distribution shifts, some of which are schematized in Fig. 2. Foreshadowing, our main finding is that distribution shifts in even low-level image attributes break DNN-based models of the visual cortex. This observation highlights a problem in modern models of the visual cortex—good predictions are limited to images that belong to the training data distribution.

To explain the OOD model-performance drop, we built on theoretical work positing that generalization performance is closely correlated with the amount of distribution shift [13, 14]. While theoretical studies have examined simplistic, simulated data, we show that a suitable metric of the size of distribution shifts can account for the OOD generalization performance of neural-encoding models.

In summary, our main contributions are threefold:

- We present *MacaqueITBench*, a large-scale dataset of neural population responses to over 300,000 images spanning multiple areas of the primate ventral visual pathway.
- We show that modern models of the visual cortex do not generalize well—simple distribution shifts can reduce neural predictivity to as low as 20% of in-distribution performance.
- We show that a simple metric of distribution shift sizes can predict OOD neural predictivity.

2 Related Work

2.1 DNN-based models of the Visual Cortex

A touchstone for visual neuroscience is the ability to predict neuronal responses to arbitrary images. On this test, DNN-based models have emerged as state-of-the-art models, best explaining neural response across species—e.g., mouse and macaque—and visual cortical areas—from the primary visual cortex (V1) to the high-level inferior temporal cortex (IT). DNN encoding models of the visual cortex are reviewed more generally in [15, 16]. Most pertinently here, these DNN-based models have been evaluated using random cross-validation (e.g., [17]), which tests IID generalization. OOD generalization in such models has been sparsely examined; we are only aware of one study [18]

comparing model fit to neural responses on two image types. Here, we systematically vary the type and degree of OOD splits to investigate how different splits lead to different generalization gaps.

2.2 Out-of-distribution generalization capabilities of DNNs

DNNs for object recognition have been documented to fail at generalizing across a wide range of distribution shifts. Such shifts include 2D rotations and shifts [19, 20], commonly occurring blur or noise patterns [11, 21–23], and real-world changes in scene lighting [24–26], viewpoints [7, 8, 24, 27–30], geometric modifications [31–33], color changes [34, 35], and scene context [36, 37].

There have been three broad approaches to address the lack of OOD generalization in DNNs: first, modifying the learning paradigm including modifying the architecture or loss function to enforce invariant representations [38–42], or using ensemble and meta-learning [43–45]; second, modifying the training data using data augmentation [46–49], or by increasing data diversity [22, 50–53]; third, scaling data up to beyond billions of data points [54–56]. Despite these efforts, OOD generalization remains an unsolved problem for deep networks.

3 MacaqueITBench: Image-response recordings from the ventral stream

We collected a large-scale dataset of neural population responses to over 300,000 images across sessions, comprising 8,233 unique natural images presented to seven monkeys over 109 sessions. In each session, a monkey maintained fixation while images were rapidly presented in random order. Each presentation was 83 milliseconds; with 83–150 milliseconds between presentations.

The images derived from published image sets [57] and photos taken in the lab and contained pictures of common objects, people, and other animals including monkeys (Fig. 1(b)). Image thumbnails are shown in Fig. 1(b)); sample images are provided in the supplement. Images belonged to over 300 semantic categories annotated by hand. A full list of categories can be found in the supplement. The large number and diversity of images allowed us to construct various OOD splits.

Neural responses were recorded on intracranial microelectrodes measuring extracellular electrical potentials (Fig. 1(c)) pre-processed to extract multi-unit spiking activity (Fig. 1(d)) [58, 59]. The analyses included 640 electrodes (12 multi-electrode arrays) recorded in nine hemispheres of seven monkeys, spanning four ventral-stream areas: V2, V4, central IT (CIT), and anterior IT (AIT), primarily sampling CIT and AIT (Fig. 1(e)). The electrodes were chronically implanted, and the responses showed stable selectivity when pooled across sessions. Nevertheless, our modeling focused on the more finely resolved within-session trial-averaged responses.

4 Constructing out-of-distribution data splits

We build on past work studying generalization under systematic distribution shifts [7, 9, 11, 38], and define the training and test distributions parametrically using image attributes. Using these parametric data distributions, we construct three kinds of train-test splits:

InDistribution (InD) splits: For each session, we created one In-Distribution (InD) split to compare with OOD generalization performance. We sampled 25% of the images at random, and held these out as the InD test set, with the remaining serving as the training set.

Attribute-based OOD splits: For concreteness, we describe OOD splits based on image contrast; splits based on the other image attributes were constructed analogously. For each session, we computed the contrast value for each image. Then, one of three strategies were employed:

- *High hold-out:* The 75th percentile of contrast values served as the cut-off. Images with contrast above the cut-off formed the test set. Remaining images formed the training set.
- *Low hold-out:* The 25th percentile served as the cut-off. All images below this served as the held-out test set. The remaining served as the training set.
- *Mid hold-out:* Images with contrast values between the 42.5th and 62.5th percentile served as the held-out test set. The remaining formed the training set.

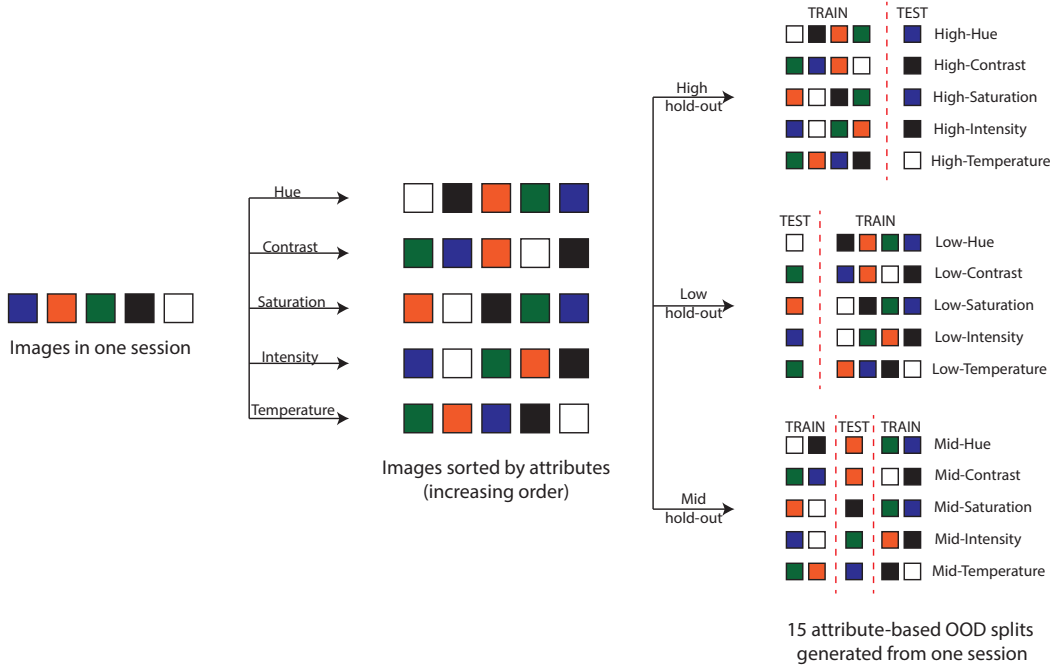


Figure 2: *Constructing multiple attribute-based OOD splits.* For each of our 109 sessions, we construct 15 different attribute-based OOD splits. These correspond to 3 hold-out strategies (*high*, *low*, *mid*) for each of 5 image-computable attributes (hue, contrast, saturation, intensity, temperature). For each attribute (e.g., hue), we compute the attribute value for each image in the session. For the *high* hold-out strategy, all images with the attribute value above a percentile cut-off serve as the OOD test set with the remaining serving as the train set. Analogously for the *low* hold-out splits, images below a percentile cut-off serve as the test set with the remaining serving as the train set. For *mid* hold-out splits, images within the middle percentiles serve as the test set.

Cosine Distance-based splits: To investigate the relationship between the size of distribution shift and neural predictivity, we constructed 3 additional test splits. We first extracted the features for every image from the pre-final layer of a pre-trained ResNet18. A random image was picked to be the seed, and all images in the session were sorted in order of increasing cosine distance between the ResNet extracted features of the images and the seed. The sorted images were then divided into three chunks based on percentile cut-offs. The first chunk corresponds to the bottom 80 percentile which served as the Training + In-Distribution Test split. A random subset of this first chunk was held out to form the In-Distribution test split, with the remaining serving as the training set. The second chunk is images in the 90th to 95th percentile, which are held-out as the *Near-OOD* test split. Finally, the third chunk corresponds to images above the 95th percentile. These are held-out as the *Far-OOD* split. To ensure a gap between the train and test distributions, we discard images between the 80th and the 90th percentile. Note that the number of images in the In-Distribution test split was kept the same number of images as the Near-OOD split.

5 Quantifying distribution shifts

We present a unified framework for measuring distribution shifts over the parametric OOD train-test splits presented in Sec. 4.

5.1 Representations for training and testing data-splits

Let $D_T = \{i_1^T, i_2^T, \dots, i_N^T\}$ denote a train split of N images, and let $D_t = \{i_1^t, i_2^t, \dots, i_n^t\}$ denote the corresponding test split of n images. $\mathcal{R}(\cdot)$ is a representation function that provides

a vector representation for an image. The train and test images thus correspond to $\mathcal{R}(D_T) = \{\mathcal{R}(i_1^T), \mathcal{R}(i_2^T), \dots, \mathcal{R}(i_N^T)\}$ and $\mathcal{R}(D_t) = \{\mathcal{R}(i_1^t), \mathcal{R}(i_2^t), \dots, \mathcal{R}(i_n^t)\}$.

We analyzed representations $\mathcal{R}(i_j)$ formed by the features extracted for an image i_j by a pre-trained DNN. We explore 8 different DNN architectures, and multiple layers for every architecture. Equations below are agnostic to the architecture and the layer used. Other alternatives could include using HOG [60] or GIST [61] image features, or the vectorized pixel values of the image.

5.2 Defining distances over different datasets

To compute the shift between $\mathcal{R}(D_T)$ and $\mathcal{R}(D_t)$, we compared three distance metrics:

Maximum Mean Discrepancy (D_{MMD}): The MMD between the two datasets can be computed as

$$D_{MMD}^2(D_T, D_t) = \frac{1}{N^2} \sum_{j=1}^N \sum_{k=1}^N K(\mathcal{R}(i_j^T), \mathcal{R}(i_k^T)) + \frac{1}{n^2} \sum_{j=1}^n \sum_{k=1}^n K(\mathcal{R}(i_j^t), \mathcal{R}(i_k^t)) - \frac{2}{Nn} \sum_{j=1}^N \sum_{k=1}^n K(\mathcal{R}(i_j^T), \mathcal{R}(i_k^t))$$

Here, $K(\mathcal{R}(i_j^T), \mathcal{R}(i_k^t))$ is a kernel distance between the representations of images i_j^T and i_k^t . A common choice for the kernel function $K(\cdot, \cdot)$ is the Gaussian RBF.

Covariate-Shift (D_{Cov}): Let $P_T(X)$ and $P_t(X)$ denote the distributions of the train and test input variables (i.e., image representations), and let $P(Y|X)$ denote the conditional distribution of the output (i.e., neural responses) given the input. Covariate shift exists if $P_T(X) \neq P_t(X)$ but $P_T(Y|X) = P_t(Y|X)$. D_{Cov} can be computed by training a binary classifier to classify if data comes from the training or the testing dataset. We denote the accuracy of this classifier as $a_{T,t}$ and measure the covariate shift as:

$$D_{Cov}(D_T, D_t) = 2 \times (0.5 - a_{T,t}).$$

Closest Cosine Distance (D_{CCD}): For every image in the test set, we find its distance to the closest training image, and compute the mean of this distance over all test images. For brevity, we will refer to this as *Closest Cosine Distance*. Let $i_k^T \in D_T$ denote the closest training image to test image $i_j^t \in D_t$ as measured by the cosine distance $D_{\cos}(\mathcal{R}(i_j^t), \mathcal{R}(i_k^T))$. The distance D_{\cos} between two vectors u and v is given by

$$D_{\cos}(u, v) = 1 - \frac{u \cdot v}{\|u\| \|v\|}$$

The average distance to the closest training image is

$$D_{CCD} = \frac{1}{n} \sum_{j=1}^n \min_{k \in \{1, 2, \dots, N\}} D_{\cos}(\mathcal{R}(i_j^t), \mathcal{R}(i_k^T))$$

6 Model training and evaluation

As depicted in Fig. 1(a), we employ a linear model to map pre-trained model activations to neuronal firing rates from the IT cortex (Fig. 1(a)). The linear model was learned using ridge regression. We used only pre-trained DNNs, not DNNs fine-tuned for our analysis.

For feature extraction, we investigated 8 DNN architectures and 2 layers for each architecture. The DNNs include supervised models trained on ImageNet (ResNet-18 [4], ViT [62]), self-supervised models trained on billion-scale data with self-supervised and weakly supervised learning

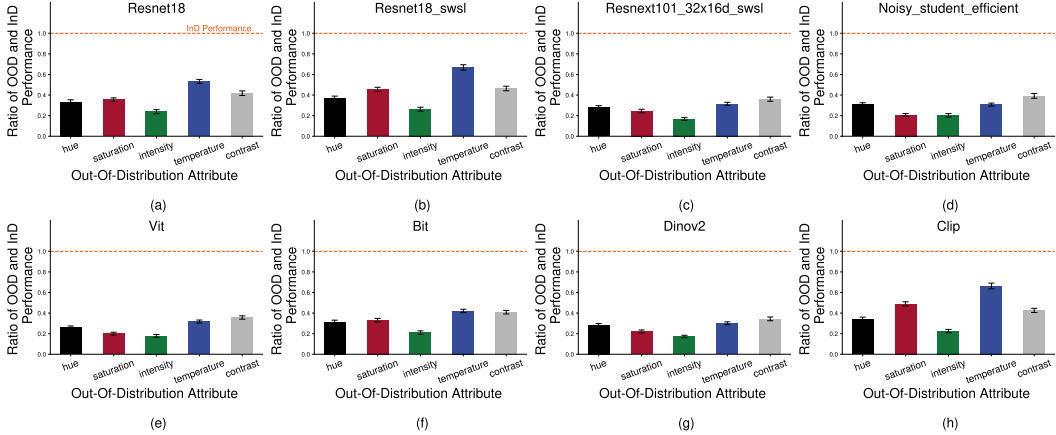


Figure 3: *Neural predictivity drops under distribution shifts.* The y-axis shows the ratio of the neural predictivity for out-of-distribution (OOD) images to in-distribution (InD) test images. A ratio of 1 would indicate no drop in performance. Each panel (a-h) shows a different architecture used for extracting image features. Each bar in a panels corresponds to a different OOD split constructed by using the *high* hold-out strategy across 5 different attributes (hue, saturation, saturation, intensity, temperature, and contrast). For all architectures and OOD splits, models fail to generalize well to OOD samples and are significantly and substantially below the 1.0 horizontal line. Image features were extracted from the pre-final layer for all architectures.

(ResNet18_sws1 [54], ResNext101_32x16d_sws1 [54], ResNet-50_ssl [54]), Noisy student with EfficientNet [63], self-supervised learning over billions of tokens (DinoV2 [56]), and the multi-modal vision-language model CLIP [55].

A linear encoding model was fit for the trial-averaged responses of each neuron in a session. The results are presented as the mean and S.E.M. across 109 sessions (7 monkeys); each session’s results is the median across neurons. The model fit per neuron was quantified as the ceiling-normalized, squared Pearson’s correlation, $r_{\text{pred}}^2/r_{\text{cons}}^2$ following convention [17, 64] and related to the explained variance, R^2 . The ceiling r_{cons} of a neuron was calculated as its response correlation between split-half trials, across images, with Spearman-Brown correction (because models fitting used all trials per image). The model fit r_{pred} was the correlation across test images between neuronal responses and model predictions. All experiments were conducted on a compute cluster with 300 nodes, 48 cores per node. CPU machines running Rocky Linux release 8.9 (Green Obsidian) were used.

7 Results

7.1 Neural predictivity drops under distribution shifts

DNN-based encoding models become worse at predicting neuronal responses under simple shifts in the image distribution. To demonstrate this, we report the ratio of neural predictivity between OOD and In-Distribution test splits ($r_{\text{ood}}^2/r_{\text{ind}}^2$). A ratio of 1 would indicate that models generalize equally well to InD and OOD test images (horizontal dashed line; Fig. 3a). In contrast, the OOD/InD performance ratios are substantially lower than 1. For instance, the black bar in Fig. 3a shows that the model’s neural predictivity was 0.33 on *high*-hue OOD images (constructed using the *high hold-out* strategy in Sec. 4) compared to images with InD hue. Models show a similar lack of OOD generalization to OOD images with regard to saturation (red bar), intensity (green bar), temperature (blue bar), and contrast (gray bar). This performance drop was observed for all eight DNNs tested (Fig. 3b-h) and ranged from a best-case ratio of 0.66 for the CLIP model generalizing to *high*-temperature OOD images to a worst-case ratio of 0.2 for the ViT model generalizing to *high*-saturation OOD images.

The lack of OOD generalization by neuron encoding models extended to models based on intermediate DNN layers, not just the penultimate layer. Fig. 4 reports OOD/InD generalization performance

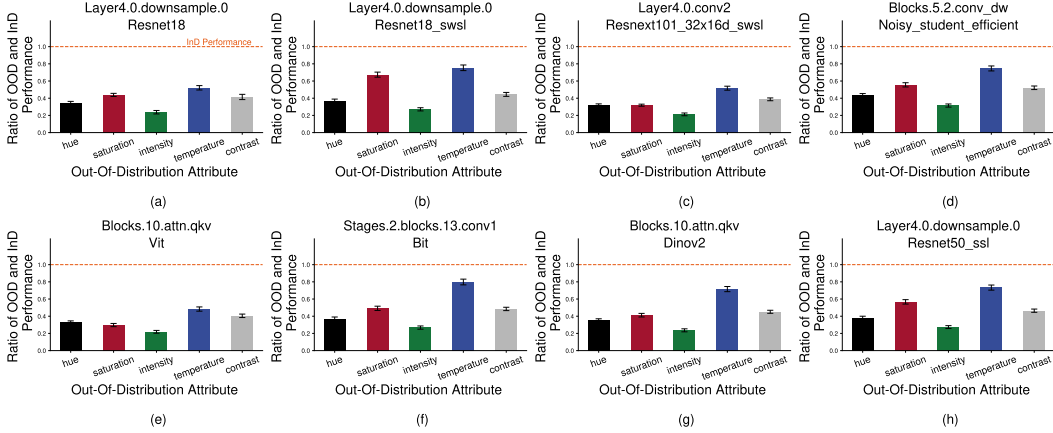


Figure 4: *Neural predictivity drops for different model layers as well.* Neural predictivity on OOD samples is reported for multiple DNN architectures across multiple different layers. Layer name is mentioned alongside architecture in all panels (a-h). All OOD splits reported here were constructed using the *high* hold-out strategy. For all architectures, layers, and OOD splits, models fail to generalize well to OOD samples and are significantly below the 1.0 horizontal line.

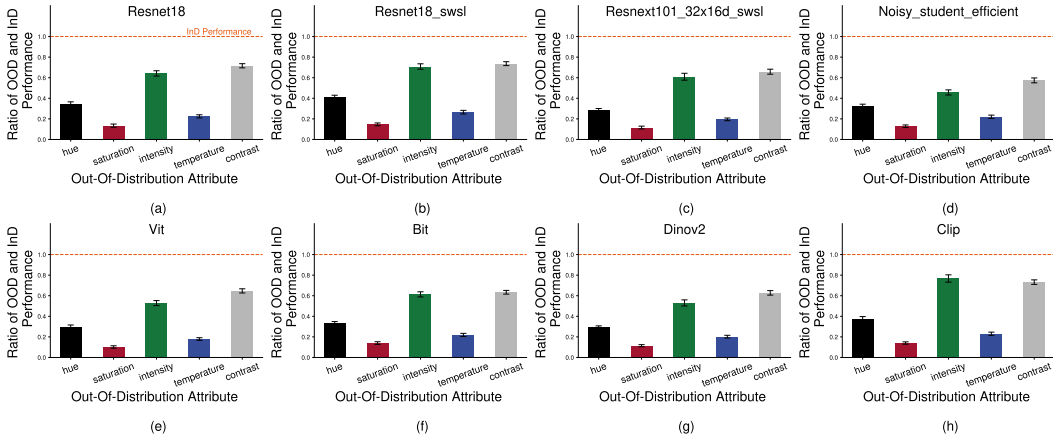


Figure 5: *Neural predictivity drops for the low hold-out strategy as well.* Neural predictivity is reported on OOD test splits constructed using the *low* hold-out strategy. Across all DNN architectures and image-computable attributes, performance is below 1.0 for all panels (a-h). Thus, models do not generalize well to OOD splits constructed with the *low* hold-out strategy as well.

ratios of models based on activations extracted from intermediate DNN layers (layer names shown in Fig. 4). For all architectures, OOD performance was substantially lower than InD performance.

The lack of model OOD generalization extended to different hold-out strategies. Fig. 5 shows the OOD/InD model performance ratio for OOD splits constructed using the *low* hold-out strategy described in Sec. 4. OOD performance was lower than InD (ratios below 1) for all architectures and image attributes. Additional results with the *mid* hold-out strategy are provided in the supplement.

Combined, these results showcase a problem for current DNN-based models of the visual cortex—despite their ability to predict neural responses to in-distribution test images, the models generalize poorly under distribution shifts even in low-level image attributes.

7.2 The distance between train and test distributions explains generalization performance

The results above raise a natural question—when and how do models of the ventral visual cortex fail to generalize under distribution shifts? Theoretical work has related OOD generalization to

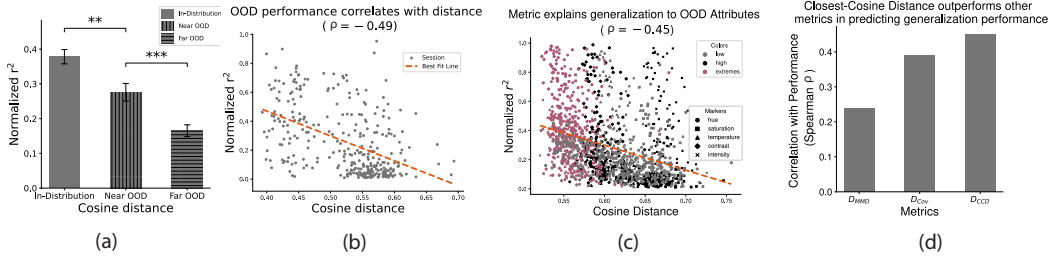


Figure 6: *Closest-Cosine Distance metric well-explains performance across all attribute-based OOD splits.* (a) Neural predictivity on distance-based splits. Models performed best on In-Distribution (InD) the split, with a dip in performance from InD to Near OOD test set (two-sided t-test, $p < 0.01$), and from Near OOD to Far-OOD (two-sided t-test, $p < 0.01$). This suggests a relationship between the extent of distribution shift and generalization performance. (b) OOD performance can be well-explained by the distribution shift. For all 109 sessions, the plot shows performance on the InD, Near-OOD, and Far-OOD with the corresponding distribution shift measured using the Closest-Cosine Distance metric (D_{CCD}). Performance and D_{CCD} have a Spearman correlation of -0.49 ($p < 0.001$). (c) Scatter plot of neural predictivity and the corresponding distribution shift (D_{CCD}) across all 15 attribute-based OOD splits for all 109 sessions. Generalization performance and the proposed distance metric have a Spearman correlation of -0.45 ($p < 0.001$) (d) Comparing different distance metrics w.r.t. their correlation with OOD performance. The proposed Closest-Cosine Distance has the highest correlation with neural predictivity, outperforming both MMD (D_{MMD}) and Covariate-Shift (D_{Cov}).

the amount of distribution shift [13, 14]. Here we apply this theoretical framework to characterize generalization in DNN models of the brain.

Intuitively, model generalization should be worse for train-test splits under larger distribution shifts. We tested this intuition by constructing splits with different levels of distribution shifts—InD, Near OOD, and Far OOD. As described in Sec. 4, images in every session were sorted based on cosine distance, and split into three chunks. The first chunk comprises the training and the In-Distribution test set, while the second and third chunks form the Near OOD and Far OOD test sets. As hypothesized, the model performance decreased progressively and significantly from In-Distribution to Near OOD, then Far OOD test distributions (Fig. 6(a); two-sided t-test, $p < 0.01$).

Beyond category-level differences, the size of the distribution shift predicted the OOD model performance drop across individual data splits (Fig. 6(b)). The distribution shift between each pair of train and OOD test distributions was quantified with the *Closest Cosine Distance* (D_{CCD} ; described in Sec. 5). The D_{CCD} strongly correlated with the OOD model performance drop (Spearman correlation $\rho = -0.49$).

The distribution shift (D_{CCD}) calculated from ResNet features also explained OOD performance for attribute based splits (Fig. 6(c)). Across all image attributes (hue, saturation, temperature, contrast, intensity) and hold-out strategies (*low*, *high*, *mid*) used to create OOD splits, D_{CCD} correlated with OOD model performance drop with a Spearman correlation coefficient $\rho = -0.45$. Compared to two other popular measures of the sizes of distribution shifts (MMD, D_{MMD} [65] and Covariate-Shift, D_{Cov} [66]; Sec. 5), our proposed Closest Cosine Distance (D_{CCD}) metric best predicted OOD model performance (Fig. 6 (d)).

8 Conclusions

These results reveal a deep problem in modern models of the visual cortex: good prediction is limited to the training image distribution. Simple distribution shifts break DNN models of the visual cortex, consistent with broader findings that the underlying DNNs are brittle to OOD shifts. Going one step further, we introduce an image-computable metric that significantly predicts the generalization performance of models under distribution shifts. This metric can help investigators gauge how well a neural model fit on one dataset may generalize to novel images.

Our findings underline an important limitation of AI models for Neuroscience. Fields like Computer Vision have responded to the issue of distribution shifts by collecting progressively larger datasets, hoping models will learn to generalize to most images [67–70] at the billion-image scale. However, it is infeasible to achieve the same scale in neuroscience—the time needed to present a billion images is already a formidable challenge, not to mention the resource intensiveness of data collection. We hope our characterization of when and how modern models of the visual cortex fail out-of-domain will motivate the development of data-efficient ways to improve DNN generalization.

9 Limitations

In this work, we have explored the impact of OOD samples on DNN-based models of the visual cortex. Our analyses have two main limitations that we hope future research can address. First, we did not fine-tune the DNNs on neural data. It is possible that training these models on the specific images and/or neural data can help improve generalization. Second, we did not explore the contributions of the images being OOD for the underlying pre-trained DNNs, as we only fit the linear encoding models on train set images and neural data. Because our images were naturalistic, it is plausible that they belonged to the training distribution of the pre-trained models we used, some of which (e.g., CLIP) having hundreds of millions of images. An interesting future direction will be to examine how the model performance is affected by using out-of-distribution images for the pre-trained DNNs. These images could include those from ImageNet-P, ImageNet-C [11], and evolved images [3].

10 Acknowledgments

This research was partially supported by NSF grant IIS-1901030. We thank Pranav Misra, Fenil Doshi and Elisa Pavarino for insightful discussions, and Harshika Bisht for design feedback on the figures. M.S.L. took the photos in the image set collected in the lab.

References

- [1] Leland McInnes, John Healy, and James Melville. Umap: Uniform manifold approximation and projection for dimension reduction. *arXiv preprint arXiv:1802.03426*, 2018.
- [2] Pouya Bashivan, Kohitij Kar, and James J DiCarlo. Neural population control via deep image synthesis. *Science*, 364(6439):eaav9436, 2019.
- [3] Carlos R Ponce, Will Xiao, Peter F Schade, Till S Hartmann, Gabriel Kreiman, and Margaret S Livingstone. Evolving images for visual neurons using a deep generative network reveals coding principles and neuronal preferences. *Cell*, 177(4):999–1009, 2019.
- [4] Kaiming He, Xiangyu Zhang, Shaoqing Ren, and Jian Sun. Deep residual learning for image recognition. In *Proceedings of the IEEE conference on computer vision and pattern recognition*, pages 770–778, 2016.
- [5] Daniel LK Yamins, Ha Hong, Charles F Cadieu, Ethan A Solomon, Darren Seibert, and James J DiCarlo. Performance-optimized hierarchical models predict neural responses in higher visual cortex. *Proceedings of the national academy of sciences*, 111(23):8619–8624, 2014.
- [6] Spandan Madan, Tomotake Sasaki, Hanspeter Pfister, Tzu-Mao Li, and Xavier Boix. Adversarial examples within the training distribution: A widespread challenge, 2023.
- [7] Spandan Madan, Timothy Henry, Jamell Dozier, Helen Ho, Nishchal Bhandari, Tomotake Sasaki, Frédo Durand, Hanspeter Pfister, and Xavier Boix. When and how convolutional neural networks generalize to out-of-distribution category–viewpoint combinations. *Nature Machine Intelligence*, 4(2):146–153, 2022.
- [8] Avi Cooper, Xavier Boix, Daniel Harari, Spandan Madan, Hanspeter Pfister, Tomotake Sasaki, and Pawan Sinha. To which out-of-distribution object orientations are dnns capable of generalizing? *arXiv preprint arXiv:2109.13445*, 2021.

- [9] Spandan Madan, You Li, Mengmi Zhang, Hanspeter Pfister, and Gabriel Kreiman. Improving generalization by mimicking the human visual diet, 2024.
- [10] Akira Sakai, Taro Sunagawa, Spandan Madan, Kanata Suzuki, Takashi Katoh, Hiromichi Kobashi, Hanspeter Pfister, Pawan Sinha, Xavier Boix, and Tomotake Sasaki. Three approaches to facilitate invariant neurons and generalization to out-of-distribution orientations and illuminations. *Neural Networks*, 155:119–143, 2022.
- [11] Dan Hendrycks and Thomas Dietterich. Benchmarking neural network robustness to common corruptions and perturbations. *arXiv preprint arXiv:1903.12261*, 2019.
- [12] Francesco Croce, Sylvestre-Alvise Rebuffi, Evan Shelhamer, and Sven Gowal. Seasoning model soups for robustness to adversarial and natural distribution shifts. In *Proceedings of the IEEE/CVF Conference on Computer Vision and Pattern Recognition*, pages 12313–12323, 2023.
- [13] Abdulkadir Canatar, Blake Bordelon, and Cengiz Pehlevan. Out-of-distribution generalization in kernel regression. *Advances in Neural Information Processing Systems*, 34:12600–12612, 2021.
- [14] Pratik Patil, Jin-Hong Du, and Ryan J Tibshirani. Optimal ridge regularization for out-of-distribution prediction. *arXiv preprint arXiv:2404.01233*, 2024.
- [15] Nikolaus Kriegeskorte. Deep neural networks: a new framework for modeling biological vision and brain information processing. *Annual review of vision science*, 1:417–446, 2015.
- [16] Daniel LK Yamins and James J DiCarlo. Using goal-driven deep learning models to understand sensory cortex. *Nature neuroscience*, 19(3):356–365, 2016.
- [17] Martin Schrimpf, Jonas Kubilius, Ha Hong, Najib J Majaj, Rishi Rajalingham, Elias B Issa, Kohitij Kar, Pouya Bashivan, Jonathan Prescott-Roy, Franziska Geiger, et al. Brain-score: Which artificial neural network for object recognition is most brain-like? *BioRxiv*, page 407007, 2018.
- [18] Yifei Ren and Pouya Bashivan. How well do models of visual cortex generalize to out of distribution samples? *bioRxiv*, pages 2023–05, 2023.
- [19] Richard Zhang. Making convolutional networks shift-invariant again. In *International conference on machine learning*, pages 7324–7334. PMLR, 2019.
- [20] Anadi Chaman and Ivan Dokmanic. Truly shift-invariant convolutional neural networks. In *Proceedings of the IEEE/CVF Conference on Computer Vision and Pattern Recognition*, pages 3773–3783, 2021.
- [21] Eric Mintun, Alexander Kirillov, and Saining Xie. On interaction between augmentations and corruptions in natural corruption robustness. *Advances in Neural Information Processing Systems*, 34, 2021.
- [22] Cihang Xie, Mingxing Tan, Boqing Gong, Jiang Wang, Alan L Yuille, and Quoc V Le. Adversarial examples improve image recognition. In *Proceedings of the IEEE/CVF Conference on Computer Vision and Pattern Recognition*, pages 819–828, 2020.
- [23] Qizhe Xie, Minh-Thang Luong, Eduard Hovy, and Quoc V Le. Self-training with noisy student improves imagenet classification. In *Proceedings of the IEEE/CVF conference on computer vision and pattern recognition*, pages 10687–10698, 2020.
- [24] Spandan Madan, Tomotake Sasaki, Tzu-Mao Li, Xavier Boix, and Hanspeter Pfister. Small in-distribution changes in 3d perspective and lighting fool both cnns and transformers. *arXiv preprint arXiv:2106.16198*, 2021.
- [25] Sara Beery, Grant Van Horn, and Pietro Perona. Recognition in terra incognita. In *Proceedings of the European conference on computer vision (ECCV)*, pages 456–473, 2018.
- [26] Qian Zhang, Qing Guo, Ruijun Gao, Felix Juefei-Xu, Hongkai Yu, and Wei Feng. Adversarial relighting against face recognition. *arXiv preprint arXiv:2108.07920*, 2021.

- [27] Andrei Barbu, David Mayo, Julian Alverio, William Luo, Christopher Wang, Dan Gutfreund, Josh Tenenbaum, and Boris Katz. Objectnet: A large-scale bias-controlled dataset for pushing the limits of object recognition models. *Advances in neural information processing systems*, 32, 2019.
- [28] Hsueh-Ti Derek Liu, Michael Tao, Chun-Liang Li, Derek Nowrouzezahrai, and Alec Jacobson. Beyond pixel norm-balls: Parametric adversaries using an analytically differentiable renderer. *arXiv preprint arXiv:1808.02651*, 2018.
- [29] Xiaohui Zeng, Chenxi Liu, Yu-Siang Wang, Weichao Qiu, Lingxi Xie, Yu-Wing Tai, Chi-Keung Tang, and Alan L Yuille. Adversarial attacks beyond the image space. In *Proceedings of the IEEE/CVF Conference on Computer Vision and Pattern Recognition*, pages 4302–4311, 2019.
- [30] Akira Sakai, Taro Sunagawa, Spandan Madan, Kanata Suzuki, Takashi Katoh, Hiromichi Kobashi, Hanspeter Pfister, Pawan Sinha, Xavier Boix, and Tomotake Sasaki. Three approaches to facilitate dnn generalization to objects in out-of-distribution orientations and illuminations: late-stopping, tuning batch normalization and invariance loss. *arXiv preprint arXiv:2111.00131*, 2021.
- [31] Amir Belder, Gal Yefet, Ran Ben-Itzhak, and Ayellet Tal. Random walks for adversarial meshes. In *ACM SIGGRAPH 2022 Conference Proceedings*, pages 1–9, 2022.
- [32] Chaowei Xiao, Dawei Yang, Bo Li, Jia Deng, and Mingyan Liu. Meshadv: Adversarial meshes for visual recognition. In *Proceedings of the IEEE/CVF Conference on Computer Vision and Pattern Recognition*, pages 6898–6907, 2019.
- [33] Dawei Yang, Chaowei Xiao, Bo Li, Jia Deng, and Mingyan Liu. Realistic adversarial examples in 3d meshes. *arXiv preprint arXiv:1810.05206*, 2:2, 2018.
- [34] Ameya Joshi, Amitangshu Mukherjee, Soumik Sarkar, and Chinmay Hegde. Semantic adversarial attacks: Parametric transformations that fool deep classifiers. In *Proceedings of the IEEE/CVF international conference on computer vision*, pages 4773–4783, 2019.
- [35] Ali Shahin Shamsabadi, Ricardo Sanchez-Matilla, and Andrea Cavallaro. Colorfool: Semantic adversarial colorization. In *Proceedings of the IEEE/CVF Conference on Computer Vision and Pattern Recognition*, pages 1151–1160, 2020.
- [36] Philipp Bomatter, Mengmi Zhang, Dimitar Karev, Spandan Madan, Claire Tseng, and Gabriel Kreiman. When pigs fly: Contextual reasoning in synthetic and natural scenes. *arXiv preprint arXiv:2104.02215*, 2021.
- [37] Mengmi Zhang, Claire Tseng, and Gabriel Kreiman. Putting visual object recognition in context. In *Proceedings of the IEEE/CVF Conference on Computer Vision and Pattern Recognition*, pages 12985–12994, 2020.
- [38] Martin Arjovsky, Léon Bottou, Ishaan Gulrajani, and David Lopez-Paz. Invariant risk minimization. *arXiv preprint arXiv:1907.02893*, 2019.
- [39] Sarah Erfani, Mahsa Baktashmotlagh, Masud Moshtaghi, Xuan Nguyen, Christopher Leckie, James Bailey, and Rao Kotagiri. Robust domain generalisation by enforcing distribution invariance. In *Proceedings of the Twenty-Fifth International Joint Conference on Artificial Intelligence (IJCAI-16)*, pages 1455–1461. AAAI Press, 2016.
- [40] Prithvijit Chattopadhyay, Yogesh Balaji, and Judy Hoffman. Learning to balance specificity and invariance for in and out of domain generalization. In *Computer Vision–ECCV 2020: 16th European Conference, Glasgow, UK, August 23–28, 2020, Proceedings, Part IX 16*, pages 301–318. Springer, 2020.
- [41] Ziqi Wang, Marco Loog, and Jan Van Gemert. Respecting domain relations: Hypothesis invariance for domain generalization. In *2020 25th International Conference on Pattern Recognition (ICPR)*, pages 9756–9763. IEEE, 2021.

- [42] Da Li, Yongxin Yang, Yi-Zhe Song, and Timothy M Hospedales. Deeper, broader and artier domain generalization. In *Proceedings of the IEEE international conference on computer vision*, pages 5542–5550, 2017.
- [43] Da Li, Yongxin Yang, Yi-Zhe Song, and Timothy Hospedales. Learning to generalize: Meta-learning for domain generalization. In *Proceedings of the AAAI conference on artificial intelligence*, volume 32, 2018.
- [44] Yogesh Balaji, Swami Sankaranarayanan, and Rama Chellappa. Metareg: Towards domain generalization using meta-regularization. *Advances in neural information processing systems*, 31, 2018.
- [45] Kaiyang Zhou, Ziwei Liu, Yu Qiao, Tao Xiang, and Chen Change Loy. Domain generalization in vision: A survey. *arXiv preprint arXiv:2103.02503*, 2021.
- [46] Hongyi Zhang, Moustapha Cisse, Yann N Dauphin, and David Lopez-Paz. mixup: Beyond empirical risk minimization. *arXiv preprint arXiv:1710.09412*, 2017.
- [47] Dan Hendrycks, Norman Mu, Ekin D Cubuk, Barret Zoph, Justin Gilmer, and Balaji Lakshminarayanan. Augmix: A simple data processing method to improve robustness and uncertainty. *arXiv preprint arXiv:1912.02781*, 2019.
- [48] Zhenlin Xu, Deyi Liu, Junlin Yang, Colin Raffel, and Marc Niethammer. Robust and generalizable visual representation learning via random convolutions. *arXiv preprint arXiv:2007.13003*, 2020.
- [49] Xun Huang and Serge Belongie. Arbitrary style transfer in real-time with adaptive instance normalization. In *Proceedings of the IEEE international conference on computer vision*, pages 1501–1510, 2017.
- [50] Shiv Shankar, Vihari Piratla, Soumen Chakrabarti, Siddhartha Chaudhuri, Preethi Jyothi, and Sunita Sarawagi. Generalizing across domains via cross-gradient training. *arXiv preprint arXiv:1804.10745*, 2018.
- [51] Fengchun Qiao, Long Zhao, and Xi Peng. Learning to learn single domain generalization. In *Proceedings of the IEEE/CVF Conference on Computer Vision and Pattern Recognition*, pages 12556–12565, 2020.
- [52] Aman Sinha, Hongseok Namkoong, Riccardo Volpi, and John Duchi. Certifying some distributional robustness with principled adversarial training. *arXiv preprint arXiv:1710.10571*, 2017.
- [53] Riccardo Volpi, Hongseok Namkoong, Ozan Sener, John C Duchi, Vittorio Murino, and Silvio Savarese. Generalizing to unseen domains via adversarial data augmentation. In S. Bengio, H. Wallach, H. Larochelle, K. Grauman, N. Cesa-Bianchi, and R. Garnett, editors, *Advances in Neural Information Processing Systems*, volume 31. Curran Associates, Inc., 2018.
- [54] I. Zeki Yalniz, Hervé Jégou, Kan Chen, Manohar Paluri, and Dhruv Mahajan. Billion-scale semi-supervised learning for image classification. *CoRR*, abs/1905.00546, 2019.
- [55] Alec Radford, Jong Wook Kim, Chris Hallacy, Aditya Ramesh, Gabriel Goh, Sandhini Agarwal, Girish Sastry, Amanda Askell, Pamela Mishkin, Jack Clark, et al. Learning transferable visual models from natural language supervision. In *International conference on machine learning*, pages 8748–8763. PMLR, 2021.
- [56] Maxime Oquab, Timothée Darcet, Théo Moutakanni, Huy Vo, Marc Szafraniec, Vasil Khalidov, Pierre Fernandez, Daniel Haziza, Francisco Massa, Alaaeldin El-Nouby, et al. Dinov2: Learning robust visual features without supervision. *arXiv preprint arXiv:2304.07193*, 2023.
- [57] Talia Konkle, Timothy F Brady, George A Alvarez, and Aude Oliva. Conceptual distinctiveness supports detailed visual long-term memory for real-world objects. *Journal of experimental Psychology: general*, 139(3):558, 2010.

- [58] György Buzsáki, Costas A Anastassiou, and Christof Koch. The origin of extracellular fields and currents—eeg, ecog, lfp and spikes. *Nature reviews neuroscience*, 13(6):407–420, 2012.
- [59] Hans Super and Pieter R Roelfsema. Chronic multiunit recordings in behaving animals: advantages and limitations. *Progress in brain research*, 147:263–282, 2005.
- [60] Navneet Dalal and Bill Triggs. Histograms of oriented gradients for human detection. In *2005 IEEE computer society conference on computer vision and pattern recognition (CVPR’05)*, volume 1, pages 886–893. Ieee, 2005.
- [61] Aude Oliva and Antonio Torralba. Building the gist of a scene: The role of global image features in recognition. *Progress in brain research*, 155:23–36, 2006.
- [62] Alexey Dosovitskiy, Lucas Beyer, Alexander Kolesnikov, Dirk Weissenborn, Xiaohua Zhai, Thomas Unterthiner, Mostafa Dehghani, Matthias Minderer, Georg Heigold, Sylvain Gelly, et al. An image is worth 16x16 words: Transformers for image recognition at scale. *arXiv preprint arXiv:2010.11929*, 2020.
- [63] Qizhe Xie, Minh-Thang Luong, Eduard Hovy, and Quoc V. Le. Self-training with noisy student improves imagenet classification, 2020.
- [64] Will Xiao, Saloni Sharma, Gabriel Kreiman, and Margaret S Livingstone. Feature-selective responses in macaque visual cortex follow eye movements during natural vision. *Nature Neuroscience*, pages 1–10, 2024.
- [65] Arthur Gretton, Karsten M Borgwardt, Malte J Rasch, Bernhard Schölkopf, and Alexander Smola. A kernel two-sample test. *The Journal of Machine Learning Research*, 13(1):723–773, 2012.
- [66] Masashi Sugiyama and Motoaki Kawanabe. *Machine learning in non-stationary environments: Introduction to covariate shift adaptation*. MIT press, 2012.
- [67] Dingshuo Chen, Yanqiao Zhu, Jieyu Zhang, Yuanqi Du, Zhixun Li, Qiang Liu, Shu Wu, and Liang Wang. Uncovering neural scaling laws in molecular representation learning. *Advances in Neural Information Processing Systems*, 36, 2024.
- [68] Ethan Caballero, Kshitij Gupta, Irina Rish, and David Krueger. Broken neural scaling laws. *arXiv preprint arXiv:2210.14891*, 2022.
- [69] Gabriele Prato, Simon Guiroy, Ethan Caballero, Irina Rish, and Sarath Chandar. Scaling laws for the out-of-distribution generalization of image classifiers. In *ICML 2021 Workshop on Uncertainty and Robustness in Deep Learning*, 2021.
- [70] Hiroki Naganuma and Ryuichiro Hataya. An empirical investigation of pre-trained model selection for out-of-distribution generalization and calibration. *arXiv preprint arXiv:2307.08187*, 2023.

Supplementary Material

List of semantic categories in MacaqueITBench

Table 1 reports a list of all semantic categories in MacaqueITBench. As can be seen, the 8,233 images correspond to over 300 categories.

bottleopener	cupsaucer	tractor	bowtie
recordplayer	corkscrew	calculator	shoe
duster	lock	scissors	gift
guitar	swissarmyknife	pda	servingspiece
ceilingfan	nunchaku	radio	socks
sushi	filingcabinet	Other	waterbottle
leaves	watergun	trumpet	Big Animate
stove	chocolate	greenplant	bones
necktie	grapes	cookpot	windchime
cassettetape	mattress	fishbowl	Non
bench	tongs	microphone	lunchbox
jacket	bonzai	bullet	fan
cheesegrater	watch	cake	stool
pasta	sword	shirt	orientalplatesetting
typewriter	backpack	babushkadolls	hat
headphone	fork	wallsconce	hookah
boot	toothpaste	Gabor	abacus
quilt	short	familiarObjects	feather
fireplace	beermug	balloon	crossbow
pen	razor	dollhouse	carabiners
lightbulb	keychain	lawnmower	Glove
broom	headband	golfbag	garbagetrash
babyplayard	manorha	skateboard	shovel
christmasstocking	cooler	exercise	wineglassfull
camera	cheese	makeupcompact	plate
gong	cellphone	showercurtain	birdcage
tricycle	carfront	sleepingbag	window
umbrella	coatrack	roadsign	breadloaf
waxseal	mathcompass	dvdplayer	Rodent
handgun	binoculars	highlighter	icecreamcones
jack-o-lantern	basket	spoon	shredder
camcorder	christmastreeornamantball	apple	Face
log	cookingpan	scrunchie	stapler
flashlight	muffler	candy	orifan
golfball	pokercard	Bird	collar
washer	baseballcards	perfumbottle	babywalker
axe	patioloungechair	banana	wig
cookie	fish hook	motorcycle	sewingmachine
toy	pizza	lamp	meat
tape	tire	decorativescreen	musicstand
crib	candleholderwithcandle	grill	battery
hammer	compass	lei	hairdryer
giftbow	wheelbarrow	keyboard	trunk
iceskates	hanger	bathsuit	pill
Hand	kettle	microscope	Big
fruitparfait	Symbol	eraser	baseballbat
cage	lightswitch	laptop	sodacan
beaker	PPE	extra	kayak
sofa	fishingpole	microwave	mailbox

snowglobe	carseat	Butterfly	corset
doll	rollerskates	Fish	frisbee
trophy	saltpeppershake	pacifier	pezdispenser
rosary	router	airplane	Cat
reportfile	soapdispenser	coffin	yarn
dumbbell	chessboard	computer	aircompressor
birdhouse	Print	pipe	hotairballoon
doorknocker	anchor	bed	cashregister
loom	lipstick	measuringtape	chair
train	remotecontrol	toaster	coffeemug
pants	pie	donut	powerstrip
seasponge	beanbagchair	bike	domino
glasses	nailpolish	cherubstatue	knife
coin	printer	mp3player	leatherman
Turtle	flag	Toy	hairbrush
ladder	bucket	bell	ringbinder
wineglass	robot	stamp	spraybottle
mushroom	dresser	peppersonplate	tent
bowlofchips	videoGameController	lantern	candybar
cracker	computermouse	cane	ambulance
toothbrush	goggle	scooter	doorknob
gamesboard	lighter	tray	backgammon
tv	sink	doorwayarch	gamehandheld
wheelchair	objects	barbie doll	coffeemaker
bagel	juice	shotglass	Mask
tablesmall	highchair	spoolofstring	helmet
horseshoe	telescope	hourglass	tweezer
ring	Misc	spicerrack	handmirror
cushion	phone	vase	woodboxsmall
bowlingpin	clock	handbag	globe
key	muffin	dynamite	strainer
checkbook	pillow	sandwich	scale
ball	sippycup	Starfish	bottle
tupperware	cigarettepack	seashell	handheldvacuum
tree	earings	vacuum	suit
bullhorn	ketchupbottle	babycarriage	necklace
fridge	nest	slinky	curlingiron
desk	suitcase	pencilsharpener	speakers
button	rug	bowl	scroll
flask	paintbrush	bill	tennisracquet
boppypillow	rollingpin	saddle	frame
handkerchief	toiletseat	slate	licenseplate
laundrybasket	easteregg	accordion	crown
circuitboard	Dog	bongo	barrel
rock	pitcher		

Table 1: Images from MacaqueITBench.

Sample Images from MacaqueITBench

Fig. 7 shows sample images which were presented to Macaques to collect responses from the IT Cortex.

Additional results with Mid hold-out strategy

In the main paper, we presented results with two hold out strategies—high and low. Here, we present results with the third hold-out strategy outlined in the paper. We refer to this as the Mid hold out strategy as samples between the 42.5 and the 67.5 percentile of every OOD attribute are held out as the test set. As shown in Fig. 8, across all architectures and OOD attributes, models suffer to generalize to OOD samples for the Mid hold out strategy.

Additional results with intermediate layers

In the main paper we presented results for models trained with intermediate layers for the high hold out strategy. Here we provide additional results with models that use intermediate layers of DNNs as feature extractors. In Fig. 9 and Fig. 10 we report results for the *low* and *mid* hold-out strategies respectively.



Figure 7: Images from MacaqueITBench.

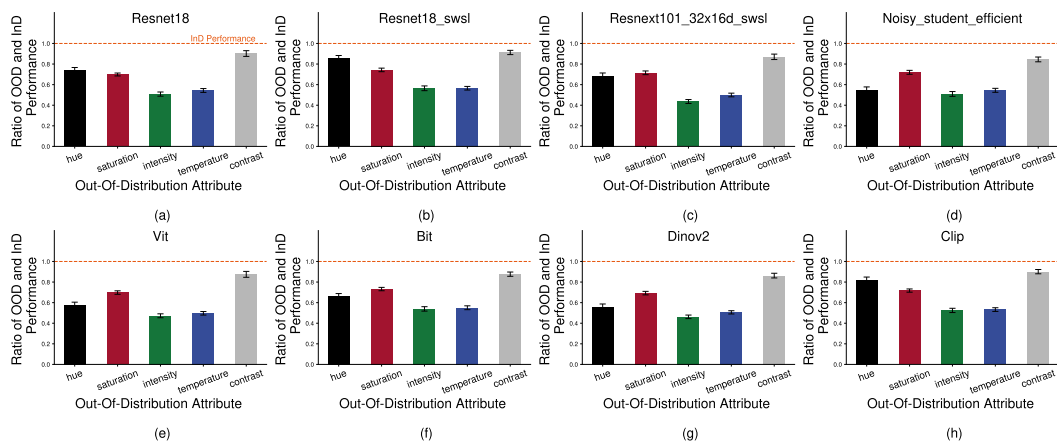


Figure 8: Neural predictivity drops for Mid hold-out strategy as well. For all architectures, across multiple OOD shifts, performance on OOD is worse than in-distribution samples for the Mid hold-out strategy as well.

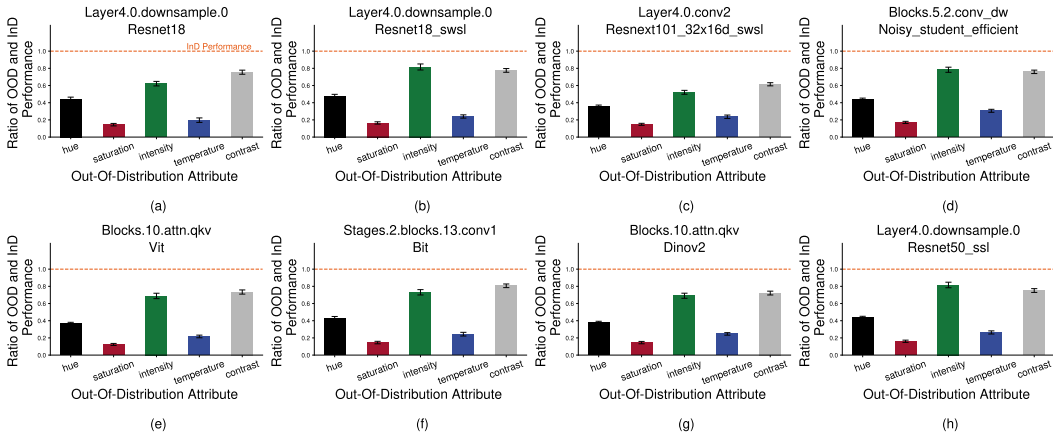


Figure 9: *Neural predictivity drops for low hold-out strategy for intermediate layer features as well.* For all architectures, across multiple OOD shifts, performance on OOD is worse than in-distribution samples for the low hold-out strategy for image features extracted from intermediate DNN layers as well.

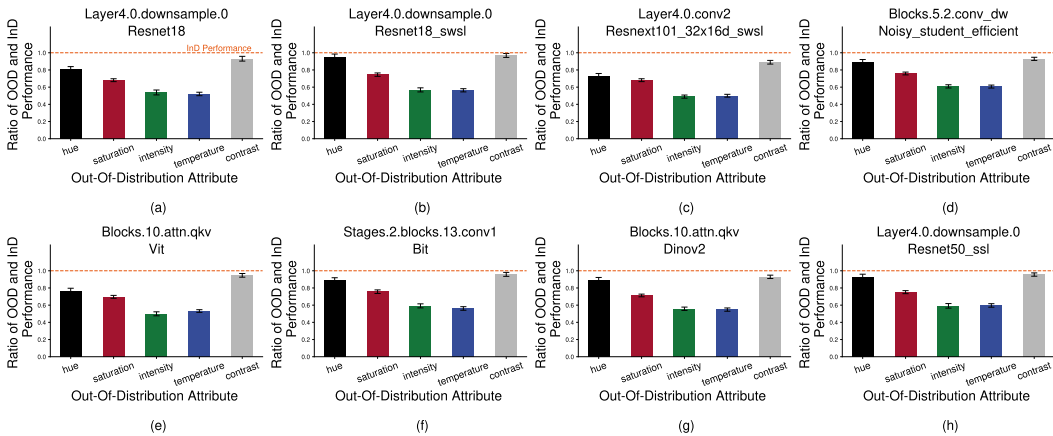


Figure 10: *Neural predictivity drops for mid hold-out strategy for intermediate layer features as well.* For all architectures, across multiple OOD shifts, performance on OOD is worse than in-distribution samples for the mid hold-out strategy for image features extracted from intermediate DNN layers as well.